DC AND RF CHARACTERISTIC OF HIGH-ELECTRON-MOBILITY TRANSISTOR (HEMT) ON AlGaN/GaN/Si FOR POWER APPLICATIONS

MOUJAHED GASSOUMI[a], A. HELALI[a], MALEK GASSOUMI[a,b*],
C. GAQUIÈRE[c], H. MAAREF[a]
[a] *Laboratory of Micro-Optoelectronics and Nanostructures (LMON), University of Monastir, 5019 Monastir, Tunisia*
[b]*College of Science, Department of Physics, Qassim University, Buraidah 51452, Saudi Arabia*
[c] *Institute of Electronics of Microelectronics and Nanotechnology IEMN, University of Science and Technology of Lille, Poincare Avenue, 59652 Villeneuve d'Ascq Cedex, France*

AlGaN/GaN/Si HEMTs grown by molecular beam epitaxy are studied with several means of characterization, the most used are direct-current and radio-frequency measurements, to see power and microwave performance of components. As has been found, the maximum of drain current achieves 0,4 A and 3,54 10^{21} cm^{-3} of 2DEG carrier concentration. Device simulation was also carried on in ATLAS to probe into the operation mechanism of GaN HEMTs and demonstrate those result. As we used this last simulation tool to extract the Radio-frequency parameter; cut-off frequency (F_t), maximum oscillation frequency (F_{max}), variation maximum stable gain (G_{ms}) and maximum available gain (G_{ma}), consequently we will know the microwave power performance and area component application.

1. Introduction

AlGaN/GaN high electron mobility transistors is a promising device for high-frequency and high-power applications [1, 2]. Gallium nitride is a great candidate for these applications because of its wide band gaps, strong spontaneous and piezoelectric polarization fields, large breakdown bias voltages and an efficient carrier transport [3].

A two-dimensional electron gas may occur at the AlGaN/GaN heterointerface with a relatively high density, following this last feature. In addition, the high concentration of carrier sheet and the strong confinement of the two-dimensional electron gas (2DEG) at the AlGaN/GaN HEMT heterointerface are appropriate for high speed applications [4].

A considerable improvement in the drain current and RF characteristics is also observed in the AlGaN/GaN HEMT [5]. In the present work reports on a study of AlGaN/GaN/Si HEMTs, we have also investigated the simulation of variation of 2DEG layer, current-voltage and the radio-frequency characteristics at output. An attempt to correlate all of the results.

2. Device structure

The AlGaN/GaN HEMTs under investigation are grown on silicon (111) substrate by using molecular beam epitaxy (MBE) (present some high purity). The sample structure is shown in Fig.1. The active layers consist in a 500 nm thick of undoped AlN/AlGaN buffer, a 1.8 μm undoped GaN channel, a 23 nm thick of undoped Al0.26Ga0.74N barrier and a 1 nm n+-GaN cap

---

*Corresponding author**: email: gassoumimalek@yahoo.fr

layer. The device processing is made following conventional HEMT fabrication steps. The ohmic contact pads are patterned using e-beam lithography. Hereafter, the metallization by means of evaporated 12/200/40/100 nm Ti/Al/Ni/Au is deposited at 900 °C during 30 s. The Schottky gate is realized using 100/150 nm Mo/Au layers with a length of 0.25 μm. The gate-source distance is 0.77μm and that of the gate-drain is 1.32μm.
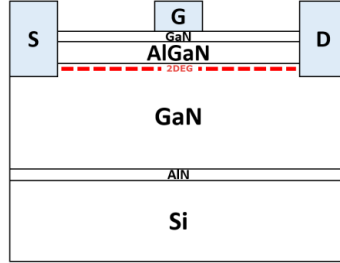
Fig. 1. Structure of AlGaN/GaN/Si HEMT

3. Physical and material models

The basic band parameters for defining heterojunctions in Blaze are bandgap parameter, electron affinity, permittivity and the conduction and valence band density of states.

3.1. Bandgap energy
Generally, the bandgap for nitrides is calculated in a two-step process: First, the band gap(s) of the relevant binary compounds are computed as a function of temperature (T) using [6]:

$$E_g(GaN) = 3.507 - \frac{0.909 \times 10^{-3} T^2}{T + 830} \tag{1}$$

$$E_g(AlN) = 6.23 - \frac{1.799 \times 10^{-3} T^2}{T + 1462} \tag{2}$$

Then, the band gap energy of $Al_xGa_{1-x}N$ ternary on composition fraction x using Vegard Law is described, where b is the bowing parameter [7]:

$$E_g(Al_xGa_{1-x}N) = xE_g(AlN) + (1-x)E_g(GaN) - bx(1-x) \tag{3}$$

We consider at 300k: Eg (AlN) =6.13 eV, Eg (GaN) =3.43 eV, b=1.3 eV.

3.2. Electron affinity
The electron affinity is calculated such that the band edge offset ratio is given by [7].

$$\frac{\Delta E_c}{\Delta E_v} = \frac{0.7}{0.3} \tag{4}$$

From this relation can be reduced expression of the electron affinity as a function of composition fraction x:

$$\chi(AlGaN) = \chi(GaN) - 1.89x + 0.91x(1-x) \tag{5}$$

3.3. Permittivity
The permittivity of the nitrides as a function of composition fraction x is given by [8]:

$$\varepsilon(Al_xGa_{1-x}N) = 8.5x + 8.9(1-x) \tag{6}$$

3.4. Density of states masses

The nitride density of states masses as a function of composition fraction, x, is given by linear interpolations of the values for the binary compounds [6]:

$$m_e(Al_xGa_{1-x}N) = 0.314x + 0.2(1-x) \tag{7}$$

$$m_h(Al_xGa_{1-x}N) = 0.417x + 1.0(1-x) \tag{8}$$

For all TCAD simulations performed in this study, the software uses different physical models, which will be used at each technological stage considered.

3.5. Shockley-Read-Hall model (recombination-generation)

The recombination rate is given by the following expression [9, 10]:

$$U_{SRH} = \frac{n.p - n_i^2}{\tau_p\left(n + n_i \exp\left[\dfrac{E_{trap}}{KT_L}\right]\right) + \tau_n\left(p + n_i \exp\left[\dfrac{-E_{trap}}{KT_L}\right]\right)} \tag{9}$$

Where E_{trap} is the difference between the trap energy level and the intrinsic Fermi level, T_L is the lattice temperature and τ_n and τ_p are the electron and hole lifetimes.

3.6. Mobility model

The low-field mobility is modeled by an expression similar to that proposed by Caughey Thomas [11]:

$$\mu_0(T, N) = \mu_{min}\left(\frac{T}{300}\right)^{\beta_1} + \frac{(\mu_{max} - \mu_{min})\left(\dfrac{T}{300}\right)^{\beta_2}}{1 + \left[N_{ref}\left(\dfrac{T}{300}\right)^{\beta_3}\right]^{\alpha\left(\frac{T}{300}\right)^{\beta_4}}} \tag{10}$$

Where T is the temperature, N_{ref} is the total doping density, and α, β_1, β_2, β_3, β_4, μ_{min} and μ_{max} are parameters that are determined from Monte Carlo simulation [11].

Another model used for high field mobility, it is based on an adjustment to the Monte Carlo data for bulk nitride, which is described by the following equation [11]:

$$\mu_n(E) = \frac{\mu_0(T, N) + \upsilon_n^{sat}\dfrac{E^{n_1-1}}{E_c^{n_1}}}{1 + \alpha\left(\dfrac{E}{E_c}\right)^{n_2} + \left(\dfrac{E}{E_c}\right)^{n_1}} \tag{11}$$

Where $\mu_0(T, N)$ is the low field mobility and the other parameters of this model are determined from Monte Carlo simulation.

4. Results and discussion

4.1. Formation of 2DEG layer

The 2DEG gas is formed at the heterostructure due to conduction band offset (ΔE_c) between the AlGaN/GaN interfaces, the combination of piezoelectric and spontaneous polarization

in these layers induce a 2DEG gas in the absence of electric field and intentional doping. It should be noted that the AlGaN/GaN HEMTs is proved to increase the mobility of carriers and reduces the alloy scattering [12, 13, 14].
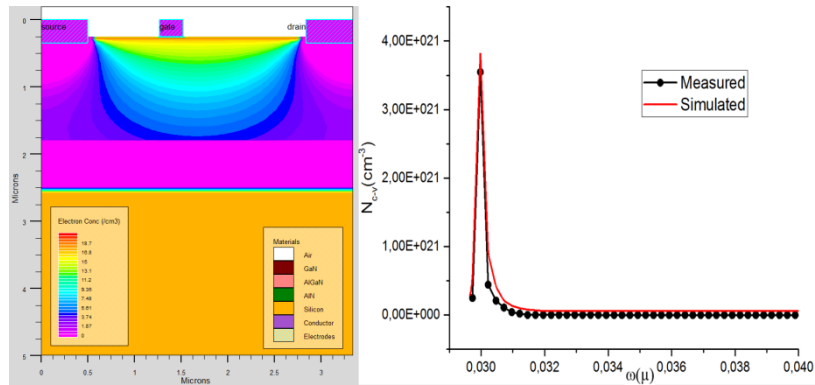
Fig. 2. Cartography, measured and simulated electron concentration of AlGaN/GaN/Si HEMT

Fig.2 shows the comparison of measured and simulated of the electron's concentration in the AlGaN/GaN/Si HEMT with the variation of the space charge width. As can be seen, the 2DEG gas is highest near the AlGaN/GaN interface. It is found about $3.54 \, 10^{21} \, cm^{-3}$ at Vgs = 0V.
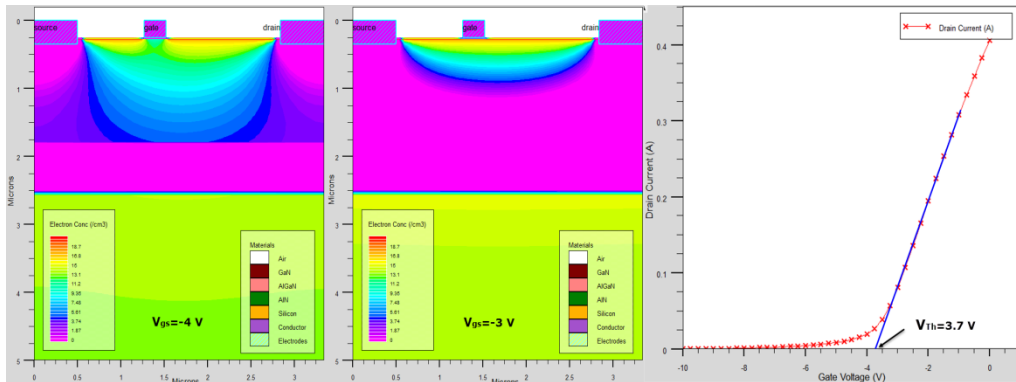
Fig. 3. Desertion of channel of AlGaN/GaN/Si HEMT

The modulation of the electron density and therefore the current in the channel is performed by steering gate voltage through the schottky contact between the gate and the AlGaN barrier layer. when Vgs is less than or equal to threshold voltage, the conduction band is located above fermi level; as we see in cartography (fig.3) carrier concentration is very low in the channel and consequently the output current is almost nonexistent. One can know the threshold voltage from the transfert characteristics Ids(Vgs) (fig.3-curve), The threshold voltage is obtained from extrapolation of the linear portion of Ids-Vgs characteristics its value is about a -3.7 V.

4.2. DC characteristics

Fig.4 showed the comparison of measured and simulated (line) drain-current characteristic as a function of drain-source voltage with the gate baised 0 to -5V steps of 1V, it is show that the simulated results fit the mesured results.
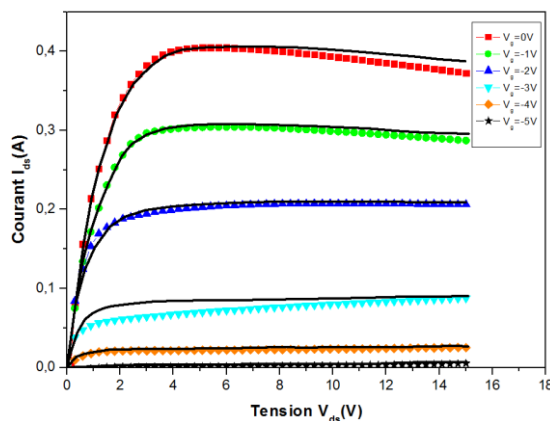
Fig. 4. Mesured and simulated output characteristic of AlGaN/GaN/Si HEMT

We observed again that the apparent saturation current exhibits a negative conductance at large Vds, it is due to the self-heating and especially results in a decrease in electron mobility. Beside to self-heating phenomenon, deep traps are also present the AlGaN/GaN heterojuction and can reduce the performance of designed HEMTs. Such trapping effects occur both at the surface and in bulk of GaN epilayer, Therefore, it is necessary to deposit a passivation layer to reduce these trapping effects [15, 16].
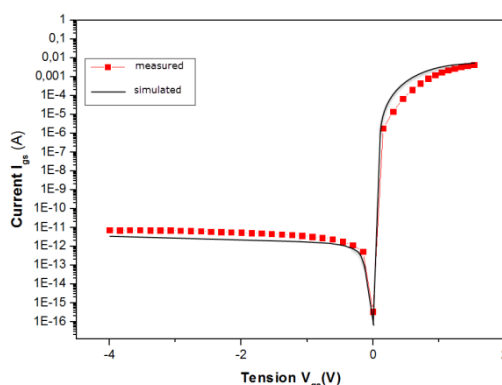
Fig. 5. Typical semilog characteristic Ig(Vg) of AlGaN/GaN/Si HEMT

In this part of paper we present the mesured and simulated current-voltage Igs(Vgs) at room temperature of AlGaN/GaN/Si HEMTs Fig.5. The study of this current can locate some defect of electrons in the active surface area, these defects are caused by surface states created by traps and dislocations accessible to the surface, in addition the absorption of ions on the surface[17].we can reduce these defects when deposed a passivation layer as SiO_2/SiN, it is decrease the inverse currents and increase the forward currents[18].

Generally, this current is dominated by the mechanism of conduction in volume and the surface as that was shown by other researchers [19, 20, 21]. The downward trend of the Schottky curve shows a decrease in the reverse leakage current of Schottky diodes and an increase in turn-on voltage.

4.3. RF characteristics

Generally, the transistor HEMTs is characterized in dynamics by tow important parameters; the cut-off frequency (FT) and the maximum oscillation frequency (Fmax). We determine these parameters from the curves of the current gain and the unilateral power gain as shonw in fig.6.
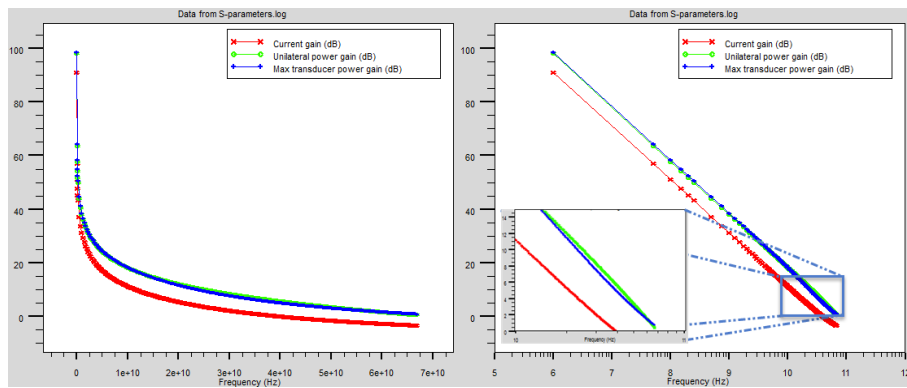
*Fig. 6. Simulated current gain (H21), Unilateral power gain (UT) and max transducer
power gain (MTG) and the typical semilog of AlGaN/GaN/Si HEMT*

The cut-off frequency is defined for the module of the current gain equal to 1(0 dB),
According to the figure, $F_T \approx 20$ GHz.

The maximum oscillation frequency characterizes the quality of the technology. It
corresponds to the maximum frequency of use of the transistor, wherein the power gain is 1 (0dB),
from to the figure, $F_{max} \approx 40$ GHz.

Another very important factor for operation in RF regime is the 'Maximum transducer
power gain' which is regarded to be the 'Figure of Merit' of any RF amplifier design. For a circuit
to operate according to the microwave regime, the power gain is considered to be a more important
factor than the voltage gain [22, 23]. Fig.6 shows the variation of this parameter, the proposed
device displays a Maximum transducer power gain of 80 dB at 20 MHz, 4,5 dB at 30 GHz and 1
dB at 50 GHz.
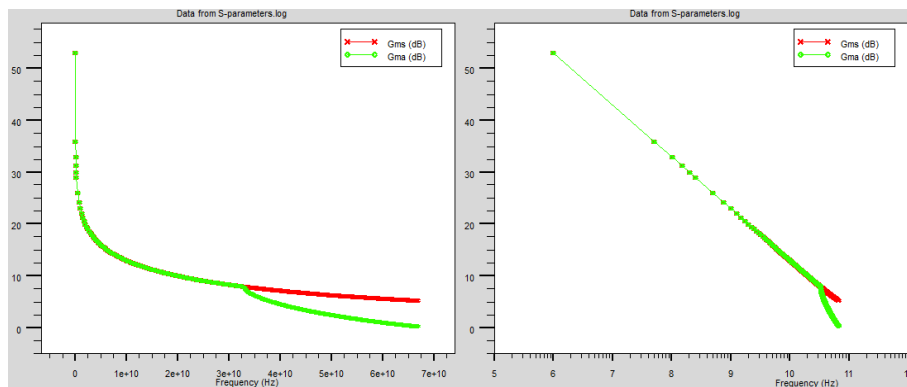
*Fig. 7. Simulated maximum available gain and maximum stable gain and the typical
semilog of AlGaN/GaN/Si HEMT*

Fig.7 shows the variation maximum stable gain G_{ms} and maximum available gain G_{ma} in
dB with frequency. Inset shows that the peak value of these tow parameters is obtained as 53 dB
and for H_{21}, UT and MTG are 91 dB, 98 dB and 92 dB through simulation respectively. A steep
decrease in G_{ms} is observed for low frequencies up to about 10 GHz. After that, the variation of
G_{ms} with frequency becomes constant until more than 60 GHz. Which indicates a good stability
performance of the for microwave and low-noise amplifier applications.

5. Conclusions

In this paper, we have presented the measured and simulated with silvaco ATLAS results of DC and AC characteristic of HEMT AlGaN/GaN on Si substrate. The device exhibited a good current of about 0.4 A, this is in addition to its properties in microwave range makes this device to use in applications operating in the Ka-band, including satellite internet and satellite space telecommunications.

References

[1] M. J. Manfra, N. Weimann, Y. Baeyens, P. Roux, D.M. Tennant, Electron. Lett. **39,** 694 (2003).

[2] V. Kumar, A. Kuliev, R. Schwindt, M. Muir, G. Simin, J. Yang, M.A. Khan,I. Adesida, Solid-State Electron. **47**, 1577 (2003).

[3] H. Morkoç, Handbook of Nitride Semiconductors and Devices, vols. I-III, Wiley-VCH, Berlin, 2008.

[4] A. Koudymov, X. Hu, K.r. J. Yang, et al., IEEE Electron Dev. **23**, 451 (2002).

[5] H. Mosbahi, M. Gassoumi, I. Saidi, H. Mejri, C. Gaquière, M.A. Zaidi, H. Maaref, Current Applied Physics. **13**, 1359 (2013).

[6] I. Vurgaftman, J.R.Meyer, M. Ram, Journal of Applied Physics, **89,** 5815 (2001).

[7] J. Piprek, Semiconductor Optoelectronic Devices: Introduction to Physics and Simulation. UCSB: Academic Press (2003): 22.

[8] O. Ambacher, et. al., J. Appl. Phys. **87**, 334 (2000).

[9] R.N. Hall, Phys. Rev. **87,** 387 (1952).

[10] W. Shockley, W.T. Read, Phys. Rev. **87**, 835 (1952).

[11] M. Farahmand, et. al., IEEE Trans. Electron Devices **48**, 535 (2001).

[12] S.B. Lisesivdin, A. Yildiz, M. Kasap, Optoelectron. Adv. Mat. **1**, 467 (2007).

[13] Y. Cao, D. Jena, Appl. Phys. Lett. **90**, 182112 (2007).

[14] I.P. Smorchkova, L. Chen, T. Mates, L. Shen, S. Heikman, B. Moran, S. Keller, S.P. DenBaars, J.S. Spech, U.K. Mishra, J. Appl. Phys. **90**, 5196 (2001).

[15] M. Gassoumi, B. Grimbert, C. Gaquière, H. Maaref, Semiconductors **46**, 382 (2012).

[16] M. Gassoumi, H. Mosbahi, A. Soltani, V. Sbrugnera-Avramovic, M. A. Zaidi, C. Gaquière, H. Mejri, H. Maaref, Materials Science in Semiconductor Processing **16**, 1175 (2013).

[17] Y. Ohno, T. Nakao, S. Kishimoto, K. Maezawa, T. Mizutani, Appl. Phys. Lett. 84 (2004).

[18] F. Jabli, M.A. Zaidi, N. B. Hamadi, S. Althoyaib, M. Gassoumi, Journal of alloys and compounds **653** 624 (2015).

[19] E. J. Miller, X. Z. Dang, E. T. Yu, Journal of Applied Physics **88**, 10(2000).

[20] S. Pandey, D. Cavalcoli, B. Frabonik A. Cavallini, T. Brazzini, F. Calle, Applied Physics Letters **100**, 152116 (2012).

[21] S. Turuvekere, N. Karumuri, A. Azizur Rahman, A. Bhattacharya, A. DasGupta, N. DasGupta, IEEE Trans. Electron Devices **60**, 3157 (2013).

[22] R. Yildirim, H. Guçlu Yavuzcan, F. V. Çelebi, L. Gokrem, Optoelectron. Adv. Mat. **3**, 781 (2009).

[23] Remzi Yildrim, Huseyin Guçlu Yavuzcan, Levent Gokrem, Technology **12**, 201 (2009).